Supporting Information

Benjamin et al. 10.1073/pnas.1310894110

SI Materials and Methods

Cancer Phenotypic Studies. Migration assays were performed in Transwell chambers (Corning) with 8-μm pore-sized membranes coated with collagen in which 50,000 cells were seeded into the top chamber and chambers were fixed and stained with Diff-Quik solutions 5 h after seeding cells per manufacturer's instructions (Dade Behring). Cells that had not migrated through the chamber on the top of the insert were removed with a cotton ball, and migrated cells were counted at a magnification of 400×. An average of cells in four fields for one migration chamber represents $n = 1$. Cell survival and proliferation assays were performed using the Cell Proliferation Reagent WST-1 (Roche) as previously described (1). Cells were washed twice in PBS, harvested by trypsinization, washed in serum-free media, and seeded into 96-well plates (10,000 cells for proliferation and 20,000 cells for cell survival) in a volume of 200 μL for 0 and 24 h before addition of WST-1 (20 μL) for 1 h at 37 °C in 5% (vol/vol) CO_2. Absorbance was then measured at 450 nm using a spectrophotometer. Invasion assays were conducted using the BD Matrigel Invasion Chambers per the manufacturer's protocol.

For soft-agar assays, growth medium (0.4 mL) containing 0.66% Bacto Agar (BD) was added to a 24-well cluster within the bottom agar layer. 231MFP or C8161 cells (4,000 cells) were resuspended in medium containing 0.375% agar (0.2 mL) and overlaid on the hardened bottom layer. Fresh medium (0.2 mL) containing 0.375% agar was added to each well once a week for 4 wk. The colonies were visualized by staining with 0.5 mg/mL 3-(4,5-dimethylthiazol-2-yl)-2,5-diphenyl tetrazolium bromide (MTT) (Sigma) for 4 h at 37 °C.

Synthesis of Alkylglyceronephosphate Synthase Substrate. We tried to also perform alkylglyceronephosphate synthase (AGPS) activity assays to confirm knockdown of AGPS activity in our cells. However, the acyl-glyceronephosphate was not commercially available, and our efforts to synthesize palmitoyl or oleoyl-glyceronephosphate failed. Nonetheless, we have described our procedures below. 1-Oleoylglycerol-3-phosphate sodium salt (5.8 mg) was suspended in 0.5 mL, and 0.05 mL dimethylformamide was added to give a slightly cloudy solution. Dess Martin periodinane (10.5 mg), two equivalents, was added as a solid, and the reaction was stirred 2.5 h at room temperature. Solvents were removed by rotary evaporation. This material was analyzed by NMR. NMR analysis showed that the olefinic protons in the oleoyl side chain had shifted from 5.348 to 5.833 ppm and the carbinol region from 3.4 to 4.2 ppm simplified significantly. Purification of the product using a 15% methanol in methylene chloride to 30% methanol/methylene chloride gave no fractions that contained the desired 1-acyldihydroxyacetone-3-phosphate or starting material. We also tried the synthesis with 1-palmitoylglycerol-3-phosphate, which was treated as follows: 1-palmitoylglycerol-3-phosphate, 22.6 mg, was diluted with 4 mL acetone, and 2 mL methylene chloride was added to give a nearly clear suspension. Solid Dess Martin periodindane, 1.58 equivalents, was added as a solid, and the reaction mixture was stirred for 1 h at room temperature. Solvent was removed by rotary evaporation. An aliquot of this solid was dissolved in methanol and submitted for analysis, but no reaction was observed by high-resolution MS.

Metabolomic Profiling of Cancer Cells. Cancer cells were grown in serum-free media for 4 h to minimize the contribution of serum-derived metabolites to the cellular profiles. Cancer cells (1×10^6 cells per 6-cm dish) were washed twice with PBS, harvested by scraping, and isolated by centrifugation at 1,400 × *g* at 4 °C, and cell pellets were flash frozen and stored at −80 °C until metabolome extractions. Nonpolar lipid metabolites were extracted in 4 mL of a 2:1:1 mixture of chloroform:methanol:PBS with inclusion of internal standards C12:0 dodecylglycerol (10 nmol) and pentadecanoic acid (10 nmol). Organic and aqueous layers were separated by centrifugation at 1,000 × *g* for 5 min, and the organic layer was collected. The aqueous layer was acidified [for metabolites such as lysophosphatidic acid (LPA) and LPA-ether (LPAe)] by adding 0.1% formic acid, followed by reextraction with chloroform. The mixture was vortexed, and the organic layers were combined, dried down under N_2, and dissolved in 120 μL chloroform, of which a 10-μL aliquot was analyzed by both single-reaction monitoring (SRM)-based LC-MS/MS or untargeted LC-MS. Metabolite separation was achieved with a Luna reverse-phase C5 column (50 × 4.6 mm, with 5-μm-diameter particles; Phenomenex). Mobile phase A was composed of a 95:5 ratio of water:methanol, and mobile phase B consisted of isopropanol, methanol, and water in a 60:35:5 ratio. Solvent modifiers 0.1% formic acid with 5 mM ammonium formate and 0.1% ammonium hydroxide were used to assist ion formation and to improve the LC resolution in both positive and negative ionization modes, respectively. The flow rate for each run started at 0.1 mL/min for 5 min to alleviate backpressure associated with injecting chloroform. The gradient started at 0% B and increased linearly to 100% B over the course of 45 min with a flow rate of 0.4 mL/min, followed by an isocratic gradient of 100% B for 17 min at 0.5 mL/min, before equilibrating for 8 min at 0% B with a flow rate of 0.5 mL/min.

MS analysis was performed with an electrospray ionization (ESI) source on an Agilent 6430 QQQ LC-MS/MS. The capillary voltage was set to 3.0 kV, and the fragmentor voltage was set to 100 V. The drying gas temperature was 350 °C, the drying gas flow rate was 10 L/min, and the nebulizer pressure was 35 psi. Representative metabolites were quantified by SRM of the transition from precursor to product ions at associated optimized collision energies. Untargeted LC-MS was performed by scanning a mass range of *m/z* 50–1,200, and data were exported as mzdata files and uploaded to XCMSOnline (xcmsserver.nutr.berkeley.edu) to identify metabolites that were differentially changed (2). These metabolites from untargeted analysis were putatively identified through using the METLIN online database (3). Standards were purchased to confirm coelution and fragmentation of the standard with the metabolite of interest. These metabolites were then quantified by SRM analysis. Metabolites were quantified by integrating the area under the peak and were normalized to internal standard values and adjusted based on external standard curves, and then levels were expressed as relative levels compared with controls. We also performed a subset of our metabolomic studies using several other internal standards representing a more diverse range of metabolites, including C13:0 LPA, C17:0/C20:4 phosphatidylcholine (PC), C13:0 lysophosphatidylcholine (LPC), C17:0/C20:4 phosphatidic acid (PA), and C17:0/C20:4 phosphatidylethanolamine (PE) and obtained very similar values to those obtained using external standard curves against dodecylglycerol and pentadecanoic acid. We have included detailed quantified data for shAGPS lines in C8161 and 231MFP cells in Dataset S1. We also performed more in-depth quantitative analysis of LPAe and LPA-plasmalogen (LPAp) species. We generated external standard curves of representative LPA, LPAe, and LPAp standards against pentadecanoic acid and C13:0 LPA standards. The limit of quantitation was determined to be 0.08 pmoles. We have provided both relative levels and absolute levels in Fig. 3*C*, Figs. S3 and S4*C*, and Dataset S1.

1. Nomura DK, et al. (2010) Monoacylglycerol lipase regulates a fatty acid network that promotes cancer pathogenesis. *Cell* 140(1):49–61.
2. Tautenhahn R, Patti GJ, Rinehart D, Siuzdak G (2012) XCMS Online: A web-based platform to process untargeted metabolomic data. *Anal Chem* 84(11):5035–5039.
3. Tautenhahn R, et al. (2012) An accelerated workflow for untargeted metabolomics using the METLIN database. *Nat Biotechnol* 30(9):826–828.

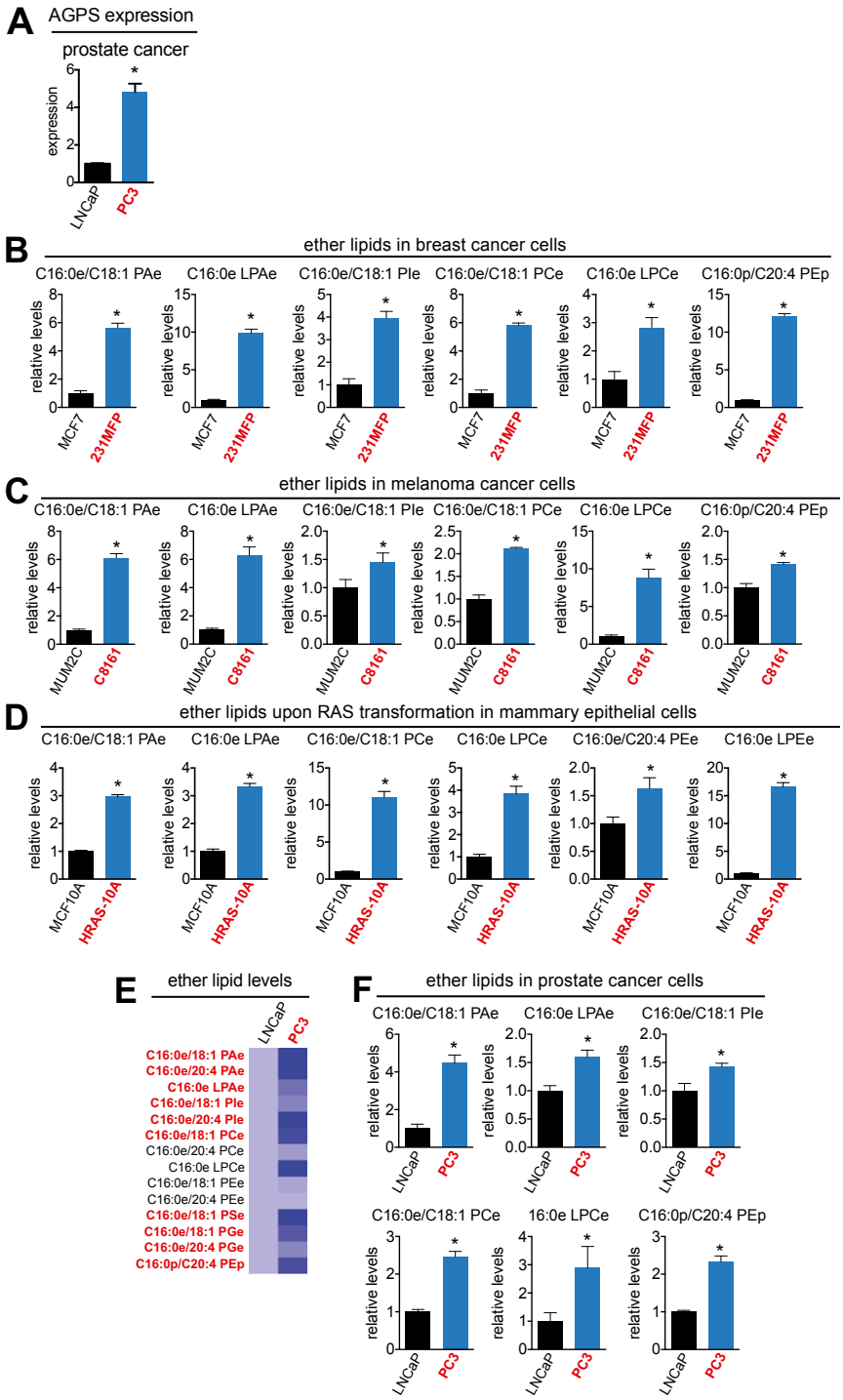

Fig. S1. AGPS expression and ether lipid levels in cancer cells. (*A*) AGPS expression is higher in the aggressive PC3 prostate cancer cells compared with the less-aggressive LNCaP cells. (*B–D*) Levels of multiple species of ether lipids are significantly higher in aggressive breast (*B*), melanoma (*C*), and Harvey-Rat sarcoma oncogene (HRAS)-transformed MCF10A (*D*) cancer cells compared with their less aggressive or control counterparts. (*E*) Several species of ether lipids are significantly higher in levels (bolded in red) in PC3 cells compared with LNCaP cells. (*F*) Several of these lipids are shown as bar graphs. Data are presented as mean ± SEM; $n = 3–5$ per group. Significance is presented as $*P < 0.05$ compared with less-aggressive or control MCF10A cells.

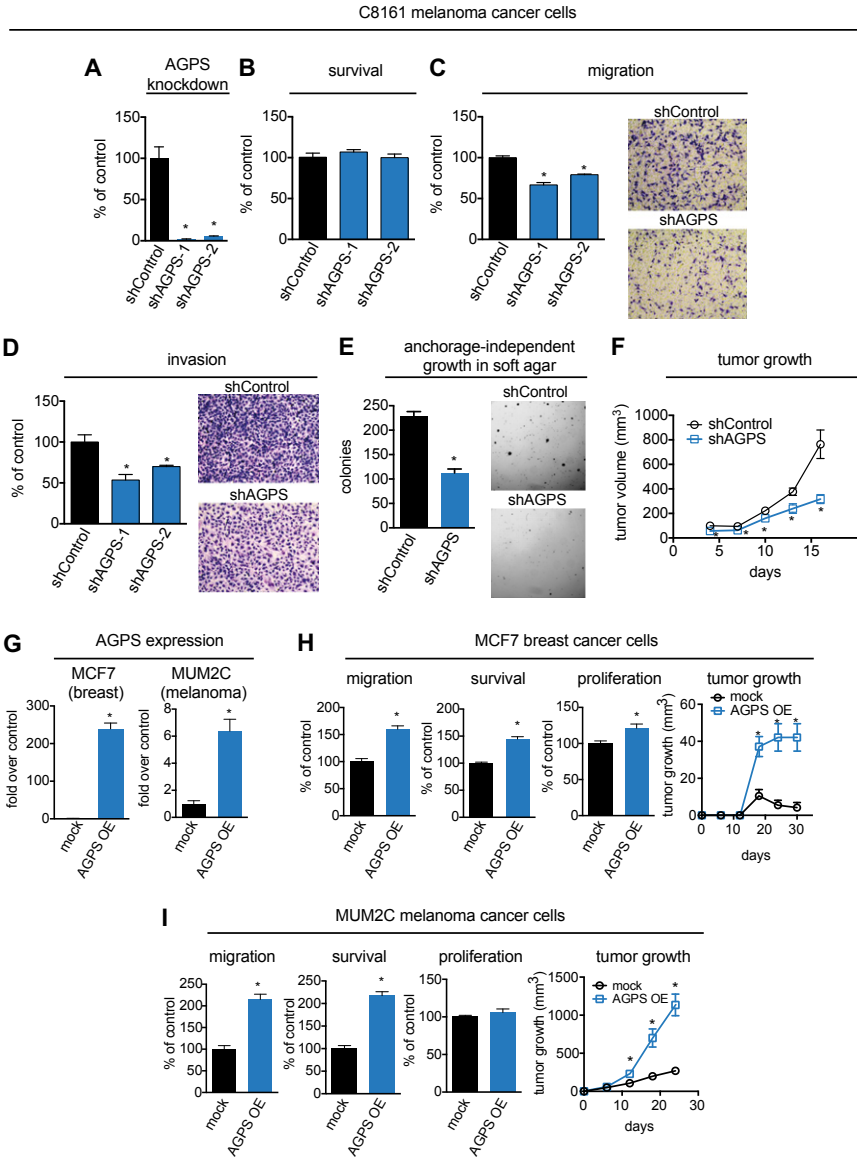

Fig. S2. AGPS ablation leads to impairments in cancer pathogenicity in C8161 melanoma cancer cells. (*A*) AGPS was knocked down in C8161 cells using two individual shRNA oligonucleotides (shAGPS-1 and shAGPS-2) resulting in >80% reduction in AGPS expression compared with shControl cells. (*B*) shAGPS-1 and shAGPS-2 show no defects in serum-free cell survival compared with shControl cells in C8161 cells. (*C* and *D*) shAGPS-1 and shAGPS-2 cells show decreased migration (*C*) and invasion (*D*) compared with shControl cells in C8161 cells (6 h). Migration and invasion assays were performed by transferring cancer cells to serum-free media for 4 h before seeding 50,000 cells into inserts with 8-μm pore size containing membranes coated with collagen (10 μg/mL) or BioCoat Matrigel, respectively. Migrated or invaded cells refer to average numbers ± SEM per four fields counted at 400× magnification. (*E*) AGPS inactivation leads to impairments in anchorage-independent growth in soft agar. (*F*) AGPS inactivation leads to impaired tumor xenograft growth in female SCID mice compared with shControl cells; 2×10^6 C8161 cells/100 μL were injected s.c. into the flank, and tumor growth was measured using calipers. (*G*) AGPS was stably overexpressed in MCF7 breast and MUM2C melanoma cancer cells. AGPS expression was assessed by quantitative PCR (qPCR). (*H*) AGPS overexpression in MCF7 cells increases migration, serum-free cell survival, and proliferation in situ, as well as in vivo tumor growth in immune-deficient SCID mice. (*I*) AGPS overexpression in MUM2C cells increases migration and serum-free cell survival in situ, as well as in vivo tumor growth in immune-deficient SCID mice. AGPS overexpression in MUM2C cells does not increase proliferation. Data are presented as mean ± SEM; $n = 3$–5 per group for *A*–*E* and *G*–*I* and 5–7 mice per group for *F*, *H*, and *I* tumor xenografts. Significance is presented as $^*P < 0.05$ compared with shControl or empty vector-infected mock controls.

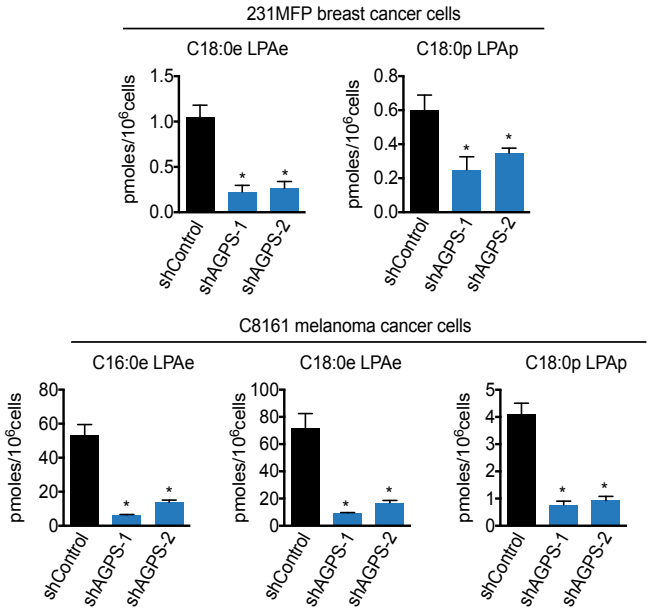

Fig. S3. Quantification of LPAe and LPAp levels in cancer cells. Shown are absolute quantification of LPAe and LPAp levels in 231MFP and C8161 shControl and shAGPS cells. Lipid levels were normalized against a C13:0 LPA internal standard and quantified against an external standard curve of LPAe/LPAp standards against C13:0 LPA. Data are presented as mean ± SEM; $n = 4–5$ per group. Significance presented as $*P < 0.05$ compared with shControl groups.

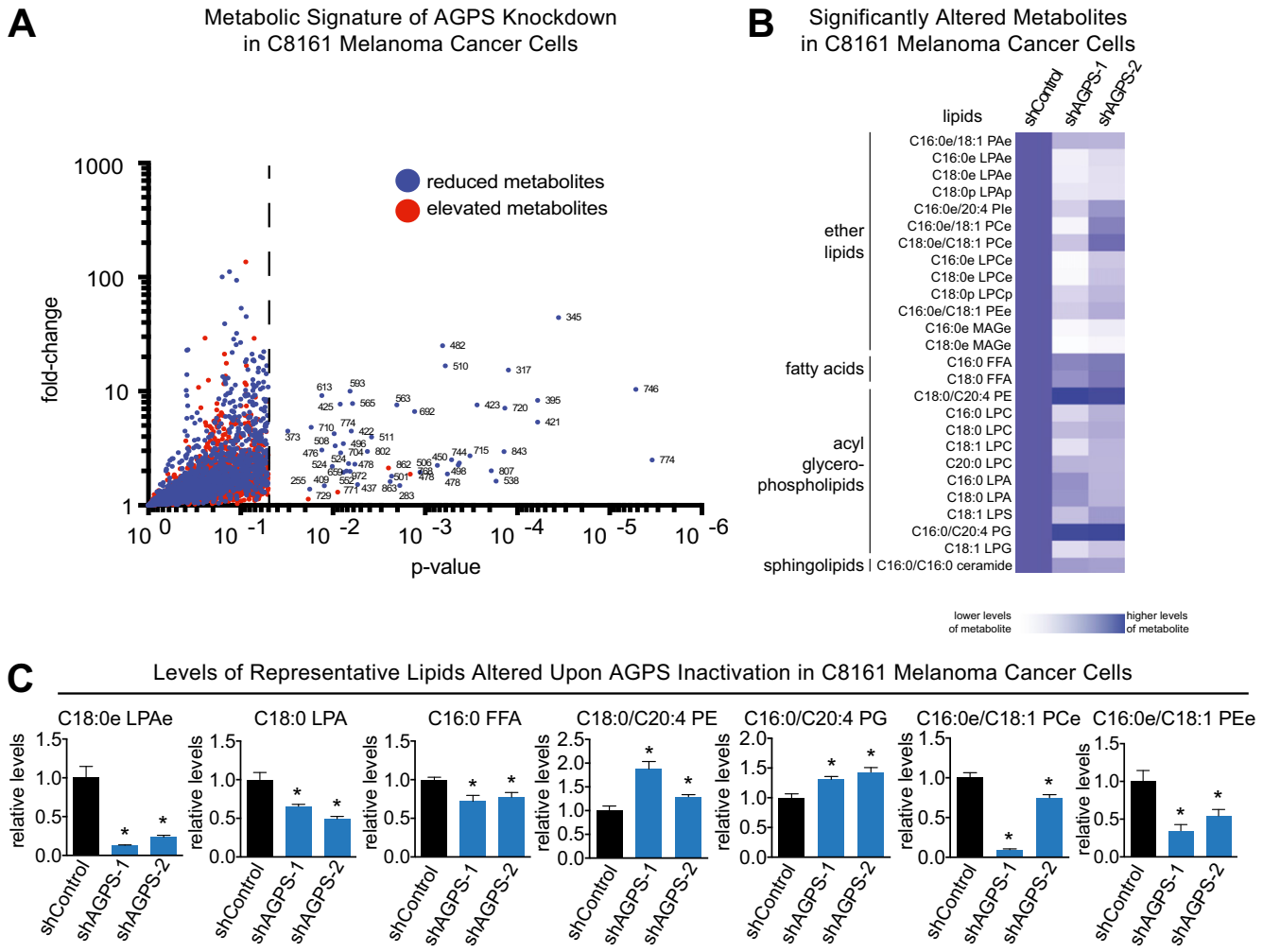

Fig. S4. Metabolomic profile of melanoma cancer cells upon AGPS inactivation. (*A*–*C*) Targeted and untargeted metabolomic analysis of AGPS knockdown in C8161 cells. (*A*) Volcano plot shows all metabolites identified by targeted and untargeted metabolomics. Blue or red dots indicate metabolites that are reduced or increased in levels upon AGPS knockdown, respectively. Metabolites that are significantly changing in levels ($P < 0.05$) between shAGPS and shControl C8161 cells are displayed to the right of the dotted line. (*B*) Heat map that shows metabolites that were significantly changing in levels in both shAGPS-1 and shAGPS-2 cells that were identified and quantified from *A*. Darker blue shading on the heat map indicates higher relative level of metabolite, and white or lighter blue color indicates lower levels of metabolite. (*C*) Representative lipids from each class are shown as bar graphs. Data are presented as mean ± SEM; $n = 4$–5 per group. Significance in *C* is presented as $*P < 0.05$ compared with shControl groups.

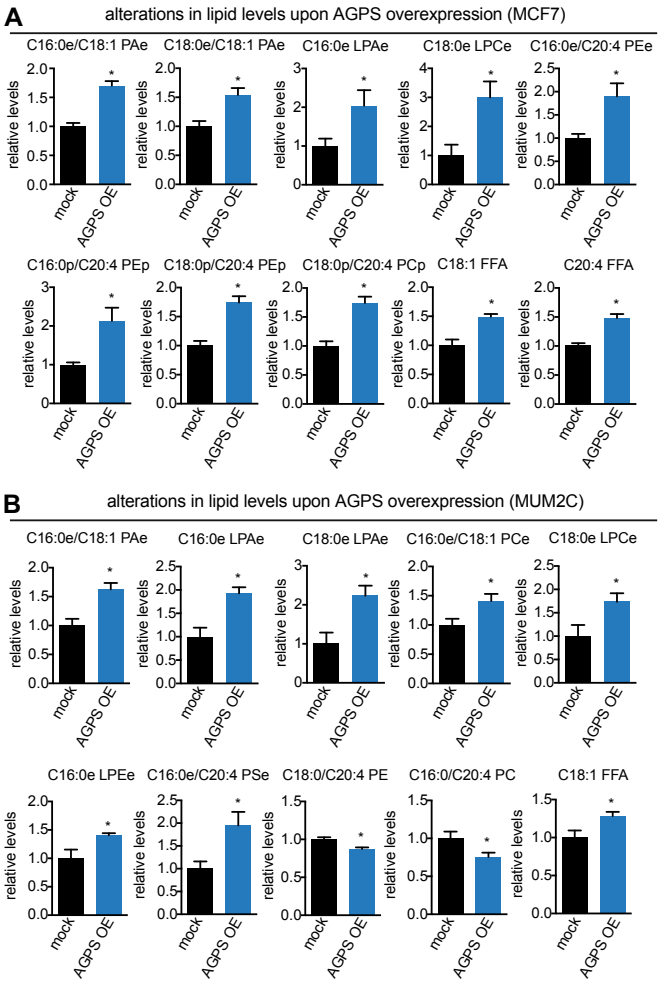

Fig. S5. Metabolite levels that are altered in AGPS overexpression breast and melanoma cancer cells. (*A* and *B*) AGPS overexpression leads to an increase in the levels of several species of ether lipids and plasmalogens, as well as an increase in certain free fatty acid (FFA) levels in breast MCF7 (*A*) and melanoma MUM2C (*B*) cancer cells. In melanoma cancer cells, we also observe a significant reduction in the levels of certain arachidonoyl-containing glycerophospholipids (*B*). Data are presented as mean ± SEM; $n = 4–5$ per group. Significance is presented as $^*P < 0.05$ compared with empty vector-infected mock groups.

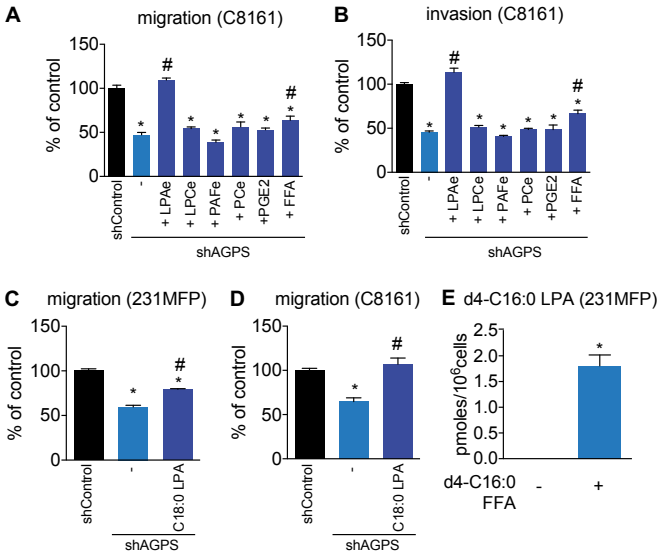

Fig. S6. Phenotypic rescue of AGPS knockdown by LPAe and palmitic acid. The migratory (*A*) and invasive (*B*) impairments in shAGPS C8161 cells are fully rescued on treating cells with low concentrations (100 nM) of C18:0e LPAe and partially rescued with palmitic acid (C16:0 FFA), but not with C16:0e LPCe, C16:0e/C20:4 PCe, C16:0e PAFe, and PGE2. (*C* and *D*) Migratory defects conferred by AGPS knockdown in 231MFP (*C*) and C8161 (*D*) cancer cells are partially or fully rescued by C18:0 LPA (100 nM), respectively. (*E*) Isotopic d4-C16:0 FFA labeling of 231MFP cancer cells (10 μM, 4 h) leads to significant incorporation of d4-C16:0 FFA into d4-C16:0 LPA. Data are presented as mean ± SEM; $n = 5–7$ per group. Significance is presented as $^{*}P < 0.05$ compared with shControl and $^{\#}P < 0.05$ comparing lipid-treated AGPS knockdown cells to DMSO-treated shAGPS cells.

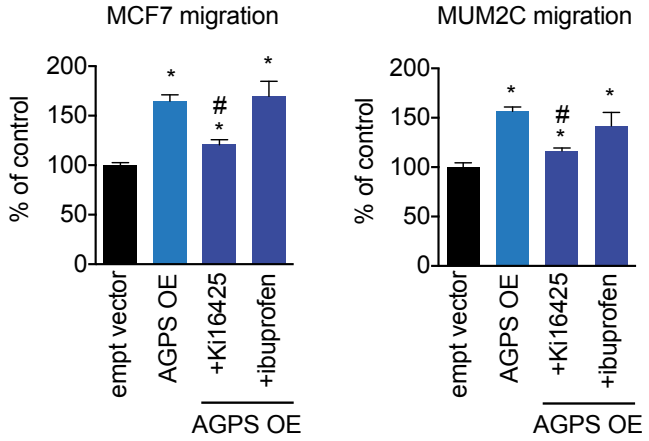

Fig. S7. Heightened pathogenic effects conferred by AGPS overexpression are reversed by an LPA receptor antagonist. The migratory increases observed on AGPS overexpression in both MCF7 and MUM2C breast and melanoma cancer cells are significantly reversed by the addition of the LPA receptor antagonist Ki16425 (10 μM), but not by the cyclooxygenase inhibitor ibuprofen (10 μM). Data are presented as mean ± SEM; $n = 3$ per group. Significance is presented as $^{*}P < 0.05$ compared with empty vector control and $^{\#}P < 0.05$ comparing drug-treated AGPS OE groups to DMSO-treated AGPS OE group.

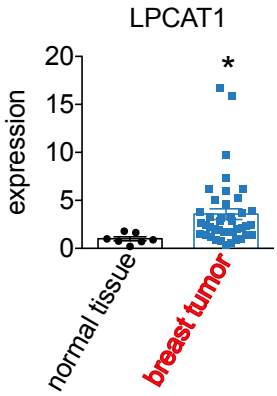

Fig. S8. LPCAT1 expression is significantly higher in primary human breast tumors. LPCAT1 expression by qPCR is significantly higher in primary human breast tumors compared with normal breast tissue. Data are presented as mean ± SEM; n = 7–20 per group. Significance is presented as $*P < 0.05$ compared with normal breast tissue.

Dataset S1. Targeted and untargeted metabolomic analysis of AGPS knockdown or overexpression in human cancer cells

Dataset S1

This spreadsheet contains all raw data for AGPS knockdown and overexpression metabolomic experiments in breast and melanoma cancer cells. Tab 1 shows the relative levels of all quantified lipids in 231MFP shControl and shAGPS cells. Tab 2 shows the absolute levels of all quantified lipids in 231MFP shControl and shAGPS cells. Tab 3 shows all metabolites and ions detected in both targeted and untargeted metabolomic analysis. Tab 4 shows the relative levels of all quantified lipids in C8161 shControl and shAGPS cells. Tab 5 shows the absolute levels of all quantified lipids in C8161 shControl and shAGPS cells. Tab 6 shows all metabolites and ions detected in both targeted and untargeted metabolomic analysis. Tab 7 shows the relative levels of all quantified lipids in MCF7 empty vector control or AGPS-overexpressing cells. Tab 8 shows the relative levels of all quantified lipids in MUM2C empty vector control or AGPS-overexpressing cells.